Journal of
Marine Science and Engineering

MDPI

Article

Field Investigation into Abrasion of Concrete at a Coastal Stepped Revetment: A U.K. Case Study

Nicholas Omoding [1], Lee S. Cunningham [1,*], Gregory F. Lane-Serff [1], Muhammad Omer [1] and Brian Farrington [2]

[1] School of Engineering, The University of Manchester, Manchester M13 9PL, UK; nicholas.omoding@manchester.ac.uk (N.O.); gregory.f.lane-serff@manchester.ac.uk (G.F.L.-S.); muhammad.omer@manchester.ac.uk (M.O.)
[2] Balfour Beatty Plc., Warrington WA3 7WD, UK; brian.farrington@balfourbeatty.com
* Correspondence: lee.scott.cunningham@manchester.ac.uk

Abstract: Although concrete abrasion damage is a major maintenance challenge for coastal structures fronted by beaches with hard coarse sediments, there are no readily available field studies that have measured abrasion damage of known concrete mixtures under defined exposure conditions. The objective of this investigation is to evaluate the abrasive exposure conditions of the concrete revetment armour units at Cleveleys on the Fylde coast of the U.K. and examine the feasibility of using terrestrial laser scanning (TLS) to measure concrete abrasion damage in field conditions. It was found that the concrete elements at Cleveleys are exposed to a macro-tidal environment, which experiences significant wave heights that vary from 0.42 to 1.92 m, whilst the peak wave periods range from 3.7 to 6.5 s. The beach sediments have a mean size of 26 mm and are moderately sorted. TLS provides a dense point cloud of abraded surfaces suitable for quantitative assessment of concrete abrasion in the field. Based on the measured abrasion depths and exposure durations, the peak concrete abrasion rates at the site varied from 3.5 to 4.5 mm/year, and severe abrasion was concentrated in the region between mean high-water springs and mean high-water neaps, wherein the highest beach levels were also found during the survey. Finally, the abraded surfaces exhibited a polished texture with no visible craters; thus, the mechanism of concrete material loss was by grinding/polishing due to rolling/sliding sediments.

Keywords: beach sediment; coastal structures; concrete abrasion; erosive wear; shingle; terrestrial laser scanning

check for updates

Citation: Omoding, N.; Cunningham, L.S.; Lane-Serff, G.F.; Omer, M.; Farrington, B. Field Investigation into Abrasion of Concrete at a Coastal Stepped Revetment: A U.K. Case Study. *J. Mar. Sci. Eng.* **2023**, *11*, 1145. https://doi.org/10.3390/jmse11061145

Academic Editor: Erkan Oterkus

Received: 8 May 2023
Revised: 24 May 2023
Accepted: 27 May 2023
Published: 30 May 2023

1. Introduction

The British coastline is approximately 16,417 km long, and of this, 2096 km is anthropogenic, i.e., formed directly by humans, such as reclaimed land and harbours. Moreover, 1043 km and 541 km of the total length is bordered by shingle (rounded gravel) and heterogeneous beaches, respectively [1]. Shingle is defined as rounded gravel or pebbles and thus has a size range of 2 to 64 mm, according to the Wentworth scale [2]. It is estimated that up to one-third of beaches in England and Wales contain shingle to some extent [3].

According to May and Hansom [1], approx. 1365 km of the British coastline is protected by some form of coastal defence structure, with 225 km of defences located at shingle beaches. This equates to approximately 15% of coastal defence structures in Britain. In conditions where coastal defence structures are fronted by shingle beaches, abrasion, which is defined here as the erosive effect of wave-driven solids, will take place to differing degrees [4]. This can inflict serious damage to concrete (the most commonly used material in modern coastal defences) as well as to masonry and timber structures. An earlier survey in Britain of 188 seawalls situated in sand, sand/rock, sand/gravel, gravel/chalk, gravel, and chalk beaches found that approximately 9% of them had suffered significant abrasion damage [5]. A later survey of 57 coastal defence structures [6] also found that the same proportion had been significantly abraded. The same survey also revealed that 8% of the 72 listed inland waterfront retaining structures exhibited abrasion.

Very few field studies of shingle-driven abrasion of concrete coastal defence structures are readily available in the literature [7]. Allen and Terret [8] investigated the relationship between concrete abrasion and cement type, aggregate properties, and mixture proportioning using 28 sloping test panels constructed at Fleetwood on the Fylde coast, one of the most abrasive environments on the U.K. coastline. After 7 years of exposure to the action of shingle transported by breaking waves, concrete abrasion depths were found to vary from 13 to 89 mm. To the best of the authors' knowledge, Allen and Terret's [8] is the only published study that has examined the issue of concrete abrasion damage in coastal conditions with quantitative details. Based on the preceding review, abrasion is a significant problem for the durability of the concrete elements located on a sizeable portion of the U.K. coastline. However, the fact that shingle beaches are also present in other parts of the world such as the USA, Japan, Canada, New Zealand, etc., [9], suggests that concrete abrasion is an important consideration globally.

1.1. Existing Methods of Field Measurement of Concrete Abrasion

There are two approaches that have been used in research to manually estimate the depth of concrete abrasion damage in field conditions, viz., the use of cast-in metal gauges and geodetic surveying. The use of the cast-in gauges entails incorporating vertical metal pins, which are initially flush with the concrete surface that is subject to abrasive action. The abrasion gauges are embedded in concrete at specific locations of interest during the manufacture of the element. After the required period of exposure, abrasion depths are determined from the heights of exposed metal pins anchored in the concrete. The field application of this method is presented in Figures 1 and 2.

Figure 1. Field measurement of concrete abrasion using cast-in metal gauges used at Fleetwood on the Fylde coast, U.K.

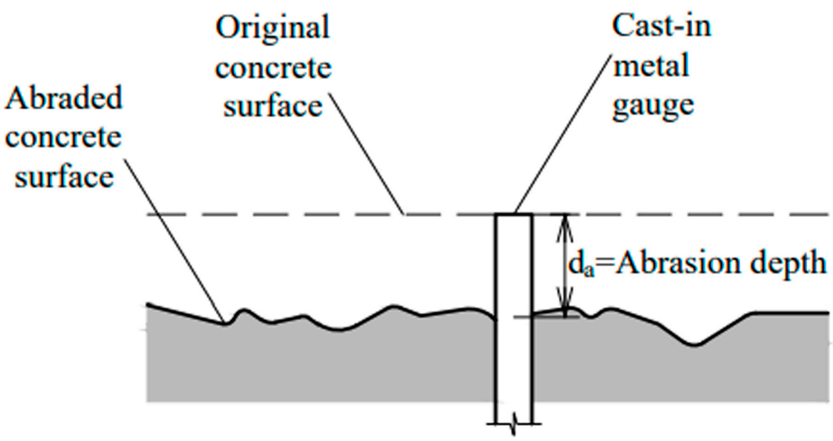

Figure 2. Schematic of abrasion measurement using cast-in metal gauges.

It can be observed in Figure 2 that the metal pins provide local benchmarks from which abrasion at specific spots can be measured. Therefore, the reliability and accuracy of this method, respectively, depend on the resistance of metal pins to damage by dislodgement and abrasion by water-transported sediments. Nevertheless, this is the approach that was adopted by Allen and Terret [8].

In contrast, Kryžanowski et al. [10] used geodetic surveying to measure abrasion damage in $2.5 \times 2.5 \times 100$ mm thick concrete test panels on the base of a stilling basin of a hydro-electric dam. The cube compressive strengths of the concretes used ranged from 22 to 73 MPa at 90 days. To determine concrete abrasion depths, 36 spot levels on a perpendicular grid of 300 mm over a 1.5×1.5 m central area of the test panels were taken before and after 2.5 years of operating the stilling basin. By comparing the corresponding spot levels taken before and after abrasion damage, it was found that concrete abrasion depths ranged from 0.2 to 0.8 mm. It was evident that a 0.5 m peripheral width was not surveyed in each test panel because abrasion in this area was thought to be greatly influenced by the stepped boundary. However, it should be noted that the study questioned the accuracy of its own method (reported to be ± 0.1 mm) because the survey found that some spots exhibited higher surface elevations after exposure to abrasion damage than the initial measurements (before abrasion).

1.2. Application of 3D Laser Scanning

In laboratory test conditions, abrasion of concrete test specimens is often defined as either percent mass or volume loss [11,12]. These losses are determined by weighing the specimen prior to and after exposure to abrasive action. The volume loss is determined from the weights of the specimen in air and water as well as density of water. Where required, the average abrasion depth can also be estimated as the ratio of material volume lost to the exposed area of the test specimen [12]. To accurately determine abrasion loss, it is recommended to weigh the concrete samples in air at saturated surface dry conditions (SSD). However, according to Hasan et al. [13], the fact that SSD is a somewhat subjective state can contribute to internal variability of the resulting volume loss estimates. To overcome this and enhance the accuracy of laboratory abrasion measurements, some studies [13,14] have recommended the use of 3D laser scanning. In this approach, a 3D laser scanner with a fixed position is used to acquire the surface characteristics of a concrete sample mounted on a turntable. Alternatively, the scanner can be robotic or hand-held and moved around to scan a stationary concrete specimen before and after abrasion damage. The point cloud acquired with such scanners is typically saved as a triangulated irregular network (TIN) surface that can be processed to provide geometric characteristics used for determining abrasion depths.

In spite of the relative success in laboratory abrasion assessment, the feasibility of using robotic or hand-held 3D laser scanners to measure abrasion in field conditions has not yet been demonstrated in the literature. However, in recent years, terrestrial laser scanners have been used successfully to rapidly acquire geometric data for purposes of bridge inspection [15,16], structural damage [17–20], and soil surface roughness [21] assessment. The findings of these studies [15–21] and relatively good laboratory results obtained with simple scanners [13,14,22] suggest that terrestrial laser scanning (TLS) is a promising technique for reliable and accurate measurement of concrete abrasion in field conditions.

1.3. Background to Terrestrial Laser Scanning

Laser scanners measure object distances by emitting a laser pulse. The distances are computed based on the principle of either ranging or triangulation depending on the scanner type. In ranging-type scanners, the distance from the transmitter to the reflecting surface is determined using either the time of flight (travel time between signal transmission and reception) or phase comparison (difference in the phase of transmitted and received waves) [23]. In contrast, triangulation scanners detect a laser spot on an object using a transmitting device and a charge-coupled device sensor, and the reflecting surface position is established from the resulting triangle [23]. The longer range provided by time-of-flight scanners makes them more preferred in engineering survey applications. Time-of-flight scanners use a set of range (R) measurements at increasing horizontal (α) and vertical (β) angles, thus generating a dense cloud of points. For each scan, the scanner automatically transforms the R, α, and β values for each raw point into three-dimensional Cartesian coordinates, i.e., (X, Y, Z), whose origin is at the scanner [23]. This principle is illustrated in Figure 3.

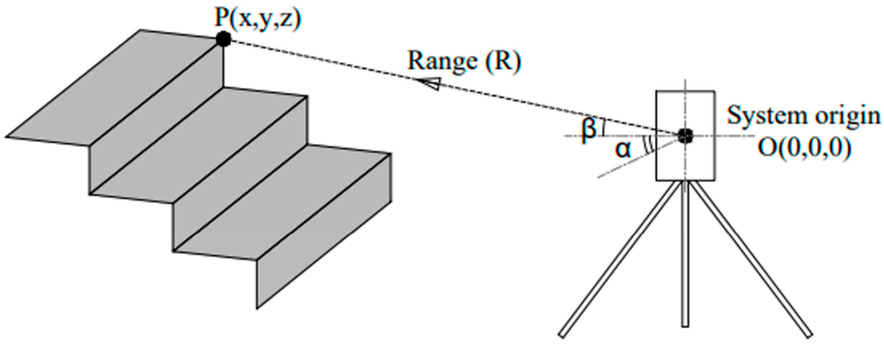

Figure 3. Illustration of the principle of a 3D laser scanner.

The range is computed from Equation (1).

$$R = \frac{1}{2}cT, \tag{1}$$

in which c is the speed of light (3×10^8 m/s), and T is the time-of-flight.

Equation (1) shows that the accuracy of range measurements from a given scanner will depend on the accuracy of the timing devices used. Besides the set of three-dimensional coordinates of each point in the cloud, scanners also provide intensity and colour (red, green, blue (RGB)) values for each data point.

TLS has been successfully used in the assessment of different forms of damage and surface deformations/changes. Mizoguchi et al. [17] used TLS to evaluate the spalling of concrete structures subject to freeze–thaw cycles. The study also presented an approach to determining the depth of concrete spalling based on the original condition. TLS was also used by Lague et al. [24] to measure surface changes in the meandering bedrock of the Rangitikei River Canyon (New Zealand), which was undergoing rapid erosion, through comparison of 3D point clouds. The study also proposed an alternative approach to point cloud comparison to determine surface change without the need for surface mesh generation, as in other existing methods. Gosliga et al. [19] developed a method for detection of post-construction deformation in bored tunnels based on field data acquired through TLS, whilst Olsen et al. [18] also used TLS data for detection of damage and analysis of volume change in full-scale structural test specimens.

In summary, the significance of concrete surface damage in hydraulic structures exposed to the abrasive action of sediment-laden flows has been emphasised in the published research. While using rudimentary methods to measure surface damage, some of these studies have presented limited quantitative data of the impact of this type of damage on the durability of exposed concrete elements. Further, 3D laser scanning has generally proven to be capable of providing reliable concrete abrasion measurements in laboratory conditions and inspection and assessment of other forms of structural damage in field conditions. However, to date and to the best of the authors' knowledge, no published studies have thoroughly investigated abrasion damage of a known concrete mixture in defined coastal exposure conditions.

Therefore, the objective of this field investigation is to (1) quantify the hydrodynamic exposure conditions of the concrete coastal structures at the selected study site; (2) examine the feasibility of using a TLS approach to investigate concrete abrasion damage in the coastal environment; and (3) using a TLS approach, quantify the rates of abrasion damage of concrete coastal defence elements.

The demonstration of the suitability of using 3D laser scanning to reliably measure concrete abrasion damage in field conditions is useful for rapid performance monitoring and planning of maintenance and/or repair of structures situated in abrasive environments. Additionally, the field abrasion and hydrodynamic data presented can be used for the calibration of future predictive abrasion models developed from laboratory tests.

The remainder of this paper is structured as follows. The study site is first described in terms of its location, construction form, and hydrodynamic conditions (sediment characteristics and wave and tidal climate). Subsequently, the methods adopted in the investigation are discussed before presenting and critically analysing the study findings. Finally, the conclusions of the study are outlined and recommendations made on areas of future research.

2. Site Description

2.1. Site Location and Selection Rationale

The study site shown in Figure 4 is at Cleveleys located on the Fylde coast of the U.K. with frontage onto the Irish Sea. The site is a modern coastal defence comprising of stepped precast concrete revetment armour units and timber groynes.

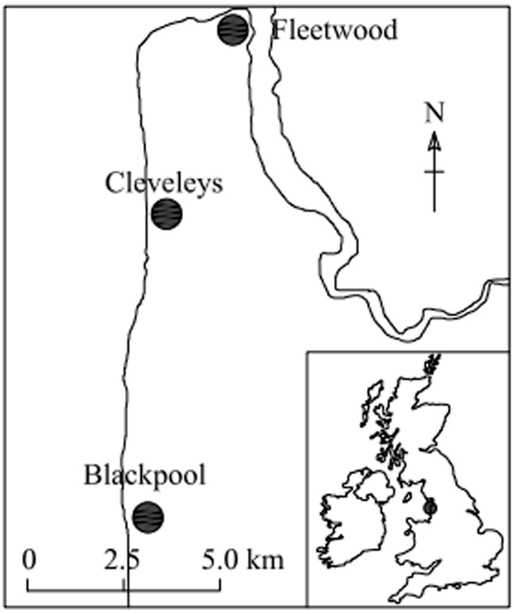

Figure 4. Location of the study site.

The site comes under the jurisdiction of the local authority Wyre Council, and the main contractor responsible for construction of the defences was Balfour Beatty. According to site documents availed by Wyre Council and Balfour Beatty, installation of the concrete armour units that were assessed commenced in March 2006 and was completed in August 2008. This particular site was chosen because (1) the concrete structures are fronted by a shingle beach, which makes it representative of the most abrasive locations in Great Britain; (2) data for the exposure environment, date of pre-cast placement, and concrete mixture used were readily available; (3) concrete surfaces have exhibited appreciable abrasion depths since installation; and (4) the site has a history of inflicting severe abrasion damage to concrete coastal defence elements, as demonstrated in Allen and Terret [8], whose study site was located just north of Cleveleys.

2.2. Description of Revetment Structure

The standard cross-section of the revetment structure over the entire coastal defence (approx. 1 km length) consists of a sloping granular soil embankment retained by sheet piling at the toe and protected by pre-cast concrete armour units in six rows, as illustrated in Figure 5. The longitudinal alignment in Figure 6 shows that scheme comprises two straight sections with three headlands marked H1, H2, and H3 and a nosed end at Rossall on its northern extent. Each of the three headlands incorporates a timber groyne, and five other groynes are distributed along the straight sections of the revetment. The general arrangement of the structure at headland H1 is presented in Figure 7.

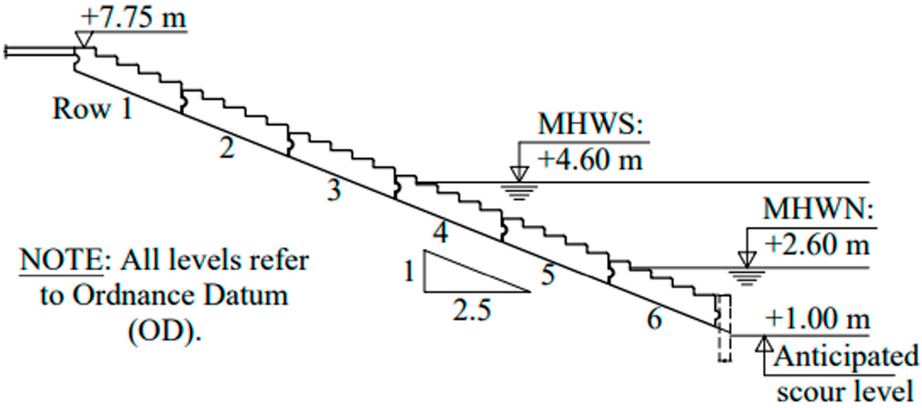

Figure 5. Cross-section showing precast concrete stepped revetment armour units based on drawings provided by Wyre Council and Balfour Beatty.

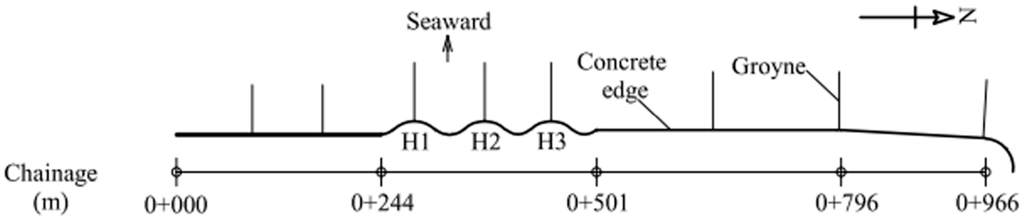

Figure 6. Longitudinal alignment of precast concrete stepped revetment armour units based on drawings provided by Wyre Council and Balfour Beatty.

Figure 7. General arrangement of the scheme (viewed from headland 1, looking south).

As shown in Figure 5, each pre-cast concrete armour unit consists of five steps with typical treads and risers of 500 and 200 mm, respectively, and the units are laid to a slope of 1 in 2.5. Further, with the exception of steps for accessing the foreshore, all armour unit steps have a nosing of 50 mm radius. The concrete units were cast up-side-down, as is standard practice for pre-cast concrete coastal defence elements [4,25,26], such that the as-struck surface that was in contact with the mould is exposed to abrasion action. This construction approach provides dense and high-quality finished surfaces that are more resistant to attack by chlorides and sulphates [25]. The concrete used had a cube compressive strength of 64.6 MPa and was selected to meet the requirements of BS 6349-1-4 [27] for structures situated in abrasive conditions. The details of the concrete mixture used were already presented and discussed in Omoding et al. [22,28].

2.3. Hydrodynamic Environment

The exposure environment of the concrete surfaces was described in terms of sediment characteristics and wave and tidal conditions based on the findings of a desk study and field sampling and analysis. The desk study comprised the collation and analysis of reports to determine the prevailing wave and tidal conditions at Cleveleys. The wave parameters reported are from a buoy [29] that was deployed on 29th June 2011 [30] at ordnance survey (OS): 321′513 E, 444′990 N, a depth of approx. 5.1 m above ordnance datum (OD). Tidal data were based on the U.K.'s National Network gauge at Liverpool, which provides tide levels with reference to chart datum [31]. It should be noted that the installation of the wave buoy occurred approx. 4 to 5 years after the concrete units were first installed.

2.3.1. Wave and Tidal Climate

The coastline at Cleveleys can be described as fetch-limited in all directions as a result of the sheltering effect provided by Ireland, the Isle of Man, and the Isle of Anglesey. For the period of June 2011 to June 2020, the site experienced significant wave heights that ranged from 0.42 to 1.92 m and peak periods of 3.7 to 6.5 s [30]. Figures 8 and 9, respectively, show roses for significant wave heights and peak periods.

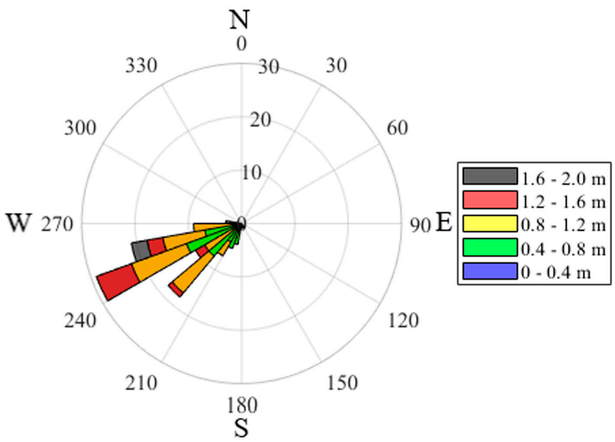

Figure 8. Rose of significant wave heights.

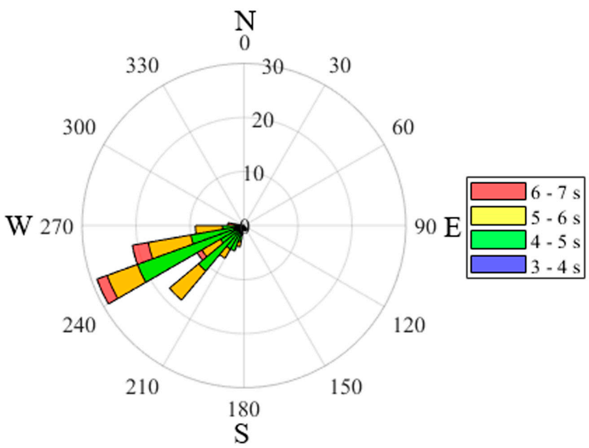

Figure 9. Rose of peak wave periods.

It can be observed from Figures 8 and 9 that a majority of the waves approached the beach from the south-westerly direction, thus obliquely to the general alignment of the revetment armour units. This approach creates longshore currents that can result in littoral drift of beach sediments.

From the classification by Davis [32], the Fylde coast is a macro-tidal environment with a mean spring tide range of 8 m that can experience storm surges of up to 1.0 m [33]. The tide levels in relation to the OD based on the tide gauge at Liverpool to the south of the site are as follows: mean high-water neaps (MHWN) = 2.6 m, mean high-water springs (MHWS) = 4.6 m, mean tide level (MTL) = 0.3 m, and highest astronomical tide (HAT) = 5.7 m.

2.3.2. Sediment Characteristics

The geological composition of the natural beach sediments at any beach is a function of the geological makeup of that area. Thus, a majority of sediments at Cleveleys originated from coastline cliffs comprised of boulder clay located north of Blackpool, while some of the pebbles were transported by glaciers from the Westmorland and Cumberland mountains [34]. As such, the shingle comprises sedimentary rocks, viz., mudstone, sandstone, limestone conglomerate, igneous rocks such as granite, as well as metamorphic rocks [1,34,35]. Further, construction activities at the coastline in the recent past have resulted in the occasional presence of concrete and brick fragments among the beach sediments.

The size characteristics of the abrasive sediments were obtained by taking samples of approximately 12.5 kg from four locations along the beach at a spacing of approximately 300 m. The samples obtained were subjected to particle size distribution analysis following the requirements of BS EN 933 [36]. Figure 10 presents the grading curves for the beach sediment samples.

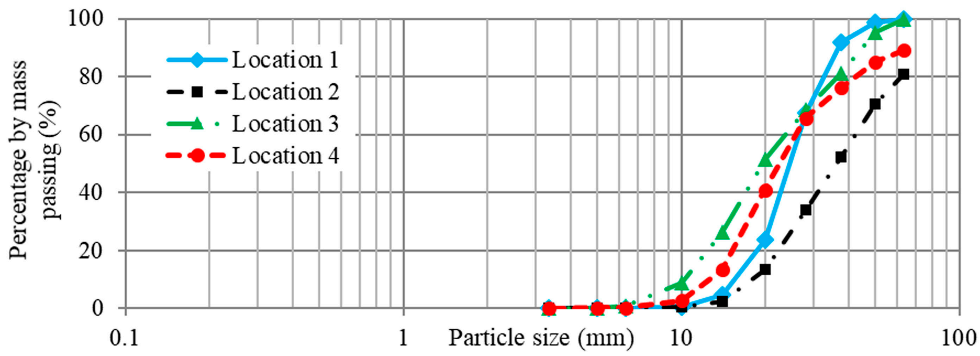

Figure 10. Grading curves for the abrasive sediments at Cleveleys.

The degree of sorting of the sediments was evaluated from Figure 10 using the size parameters, viz., D16, D50, and D84 [37], of the four sample locations. The results of this evaluation are summarised in Table 1.

Table 1. Particle size parameters for the abrasive sediments at Cleveleys.

Location	Particle Size (mm)			Degree of Sorting
	D_{16}	D_{50}	D_{84}	D_{84}/D_{16}
1	17.6	24.8	34.4	2.0
2	20.9	36.3	-	-
3	11.6	19.7	40.1	3.5
4	14.6	22.9	48.4	3.3
Mean (SD) *	16.2 (4.0)	25.9 (7.2)	41.0 (7.0)	2.9 (0.8)

* SD denotes standard deviation.

According to Rogers et al. [37], shingle beaches typically have values of median size (D50) ranging from 10 to 40 mm. Further, the degree of sorting of particles can be assessed from the ratio of D84 to D16, whereby well-sorted and well-mixed samples are those with ratios of less than 2 and greater than 16, respectively. Therefore, from the mean value of D50 of 25.9 mm and degree of sorting of 2.9 shown in Table 1, the sediments abrading the concrete revetment armour units at Cleveleys can generally be categorised as moderately-sorted shingle. Beaches with such sediments tend to exhibit slopes of 1:10 and slopes less than 1:40 on the shingle and sand sections, respectively [37]. The typical beach profile at Cleveleys, moving seaward from the visible toe of the revetment, consists of shingle at an approximate 1:10 slope for 10–20 m, which then gives way to sand and shingle at an approximate 1:60 slope. For a detailed description of the bathymetry of the site, readers are referred to the study by [38]. The range of beach slopes at Cleveleys and their impact on the location of abrasion damage is examined in more detail in Section 4.2.4.

3. Methodology

In this study, a 3D laser scanner was used to acquire data that were subsequently processed to determine the depths of abrasion damage in stepped concrete revetment armour units. The application of this method is detailed in the proceeding sub-sections.

3.1. TLS Approach

TLS was used to measure the concrete abrasion depths at three selected concrete revetment locations shown in Appendix A (Figure A1) using a Leica ScanStation P40 in Figure 11. This scanner can acquire up to 1,000,000 points per second with accuracies of ±3 and ±6 mm for scanned objects located at distances of 50 and 100 m, respectively, from the scanner [39]. The detailed specifications of the scanner are summarised in Appendix A (Table A3). In all the three locations, the scanner was set to acquire data at a high resolution.

Figure 11. Leica Scan Station P40.

3.1.1. Scan Data Processing

Once the field data acquisition was completed, the raw point cloud required processing to distil the relevant information for the creation of digital models of abraded surfaces and consequently determine abrasion depths. This was achieved using several applications, viz., Leica Cyclone Register 360 [40], Autodesk Recap 2020, AutoCAD 2020, and Cloud Compare v2.11.0 [41]. Cloud Compare is an open-source software used for analysis of point clouds. For each location investigated, the acquired point clouds from different scan stations were imported and registered in Leica Cyclone Register 360 using the visual alignment approach. After scan registration, irrelevant points such as nearby buildings, steel railings at access steps, timber groynes, etc., were cropped out and manually deleted in Autodesk Recap 2020 such that a clean point cloud for a single concrete unit was used in the analysis. Table 2 shows the total number of points and scan stations used for each concrete unit analysed for the respective location. Subsequently, the processed point cloud of the selected revetment armour unit was exported from Autodesk Recap 2020 as a .PTS file, which is compatible with Cloud Compare.

Table 2. Point cloud sizes.

Location	No. of Points in One Unit	No. of Scan Stations Used	Plan Geometric Description
P	32,773	5	Curved unit
Q	725,611	4	Curved unit
R	705,589	5	Straight unit

3.1.2. Abrasion Depth Determination

This stage of analysis aimed to compute the depths of concrete abrasion based on positions of individual points in the cloud and the meshed theoretical model of the concrete surface (prior to abrasion damage). The theoretical mesh surface model was developed within the 3D modelling suite in AutoCAD 2020 using geometric information extracted from the as-built pre-cast unit drawings supplied by Wyre Council. Thereafter, mesh surface models in .DWG file formats were imported into Cloud Compare via Autodesk 3ds Max 2020, in which models were saved as meshes with a quadrilateral polygon size of 0.2% (.OBJ file format), which can be analysed in Cloud Compare. The mesh properties for the concrete surfaces at the selected locations are summarised in Table 3.

Table 3. Mesh properties of theoretical surface models.

Unit Type	X (m)	Y (m)	Z (m)	No. of Faces	No. of Vertices
Straight	3.975	1.000	2.500	558,900	149,815
Curved	2.549	1.000	4.682	737,941	369,721

In Cloud Compare, the imported point cloud and mesh surface were aligned in the horizontal (X–Y) and vertical (Z) directions using a minimum of four common points. These reference points were located at the edges of the concrete units at the riser-tread intersection. For the concrete units on row four and five, these intersections were taken at the start of the second and fourth steps, respectively, because no severe abrasion damage was observed in these locations. Concrete abrasion depth was thus determined by Cloud-to-Mesh (C2M) comparison. C2M distance (LC2M) is computed as the distance between each point and the mesh along the local normal of the mesh surface [41].

3.2. Validation of TLS Approach

The validity of the proposed workflow and accuracy of the scanner used in the investigation were evaluated from a scan of a section of a straight concrete revetment unit situated in row 1 (the topmost row) and hence rarely reached by the tide. This unit had not suffered significant abrasion because there was no severe coarse aggregate exposure. The first stage compared the tread and riser dimensions determined from the analysis of the acquired point cloud and those from the theoretical model. Thereafter, the deviations of the point cloud from the theoretical surface profile were evaluated. Figure 12 shows the point cloud of the region of interest comprised of 496,477 data points, while the dimensions assessed are shown in Figure 13.

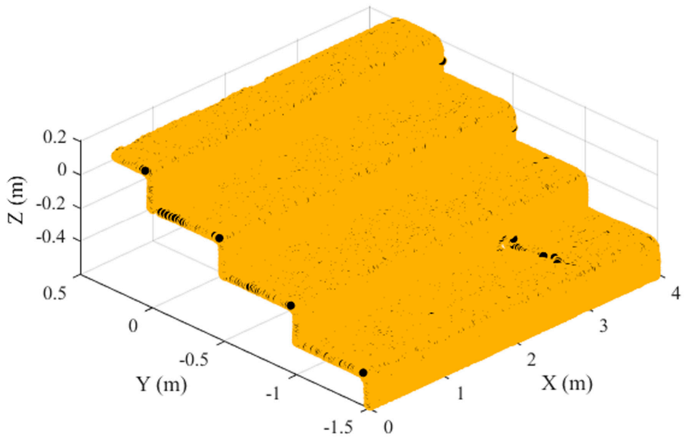

Figure 12. Scatter plot of the point cloud for the reference (unabraded) unit.

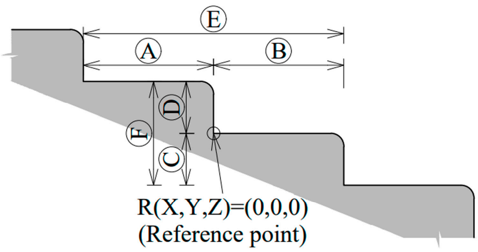

Figure 13. Dimensions assessed for TLS approach validation.

Table 4 shows measurements obtained together with percent differences between the TLS dimensions and theoretical values (Δ). The number of points from which the measurements were determined is also presented.

Table 4. Dimensions assessed for method validation.

Dimension (See Figure 13)	No. of Points Used	Measurement by TLS (mm)	Δ (%)
A	42,980	498.9 ± 1.4	0.2
B	45,447	501.0 ± 1.3	−0.2
C	130,845	204.8 ± 1.1	−2.4
D	112,222	195.9 ± 1.2	2.1

The results in Table 4 show that data acquired by TLS were capable of providing accurate measurements of the dimensions marked A to D since the mean values obtained differed from theoretical values by less than 2.5%. The accuracy significantly improved for dimensions E and F (i.e., A + B and C + D, respectively), in which the respective variations in mean values were 0.01% and 0.2%. The relatively high variations exhibited in dimensions A to D are attributable to systematic errors when selecting the reference point R, as shown in Figure 13, from which all the distances were measured.

Further, the position of each point in the cloud relative to the theoretical (unabraded) surface model was also examined. This was carried out to determine whether or not the deviation of the point cloud from theoretical surface model would be negligible, i.e., no significant abrasion of the surface.

The results of the evaluation based on 496,477 points revealed that the point cloud deviated by up to −15.7 mm (below) and +37.8 mm (above) from the reference surface. However, a quick examination of the distribution of these deviations revealed that a majority of points appeared to be within the range of ±10 mm. Based on this distribution, a numeric band filter was applied to exclude the highest 2.5% and the lowest 2.5% of the surface points. The scatter plot of 95% of the remainder of the points (471,667) is presented in Figure 14, whilst the distribution together with the normal distribution fit of the abrasion depths is shown in Figure 15. It should be noted that 95% of the points were used for consistency with the 95% confidence level typically used in establishing the characteristic strength of materials in structural design [42].

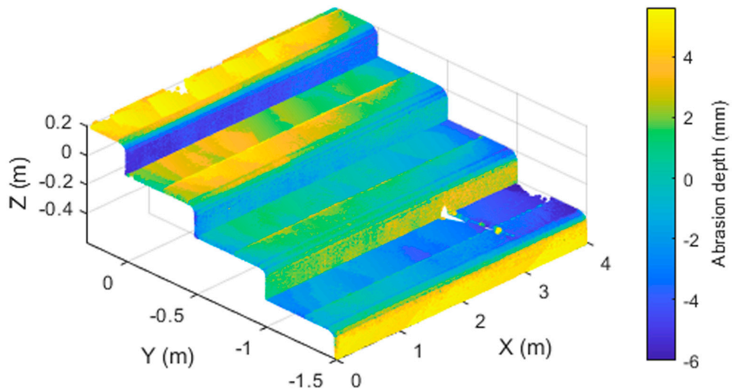

Figure 14. Scatter plot of abrasion depths after filtering the top and bottom 2.5% of data points.

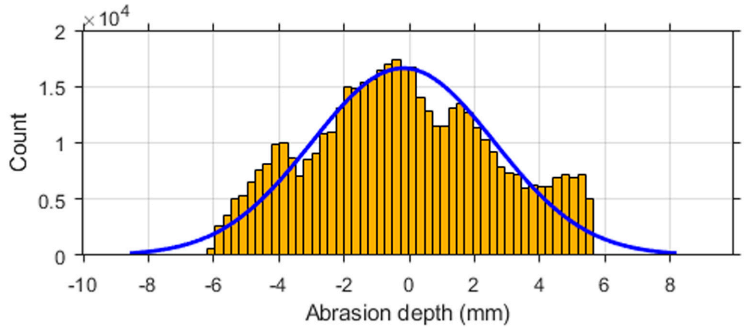

Figure 15. Distribution of filtered point cloud deviations from the theoretical surface.

As observed in Figure 15, abrasion depth values varied −6.0 mm (below) to +5.6 mm (above) from the reference surface. The magnitude of the extreme values obtained suggests that 95% of the points acquired were generally within the range of ±6 mm. This deduction is consistent with the 3D position (point) accuracy of the P40 scanner that is reported to range from 3 to 6 mm depending on the scanned object's distance from the scanner. Gyetvai et al. [15] also carried out a comparison of cross-sectional areas of structural steel sections estimated from TLS with the standard areas in the library and found that although the deviations varied from 1.4 to 30.7%, a majority of them were less than 8%. Therefore, the TLS equipment and workflow used appears to be more reliable when the concrete abrasion damage being measured is significantly greater than 6 mm. Given the date of installation and from the visual inspection, it was expected that the lower units in the inter-tidal zone would exhibit abrasion depths far in excess of 10 mm. The procedure that is demonstrated herein was therefore used to assess the abrasion damage of the concrete units at Cleveleys after carrying out the visual inspection.

4. Results and Discussion

4.1. Visual Field Observations

This stage of the study entailed recording general observations of concrete abrasion damage, concrete abrasion mechanisms, as well as the effects of other coastal structures such as timber groynes on concrete abrasion patterns.

4.1.1. General Observations

Visual observations along the entire length of the scheme were made during the site reconnaissance carried out on 25 April 2019 and an additional inspection undertaken in August 2020. It was evident that although rows 1 and 2 (i.e., the uppermost rows) of the revetment units generally did not suffer serious abrasion damage, in comparison with the appearance recorded in June 2013 (Figure 16), thus far, only the removal of the surface cement/sand matrix had occurred. The absence of this layer resulted in very slight exposure of concrete coarse aggregates (CA), characterised by the dark-coloured surface spots observed in August 2020 (Figure 17).

Figure 16. Row 1 unit (straight section) without coarse aggregate exposure.

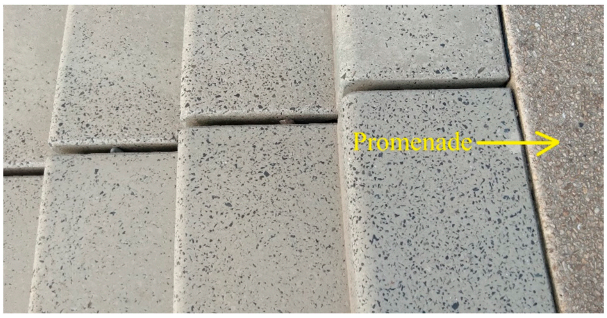

Figure 17. Row 1 units (curved section) with exposed coarse aggregates.

Closer qualitative examination of the progression of surface damage in row 1 units in Figure 18 reveals that the degree of CA exposure is greatest at the nosing of the steps followed by the treads, thus representing severe exposure zones. In fact, expectedly, at the perpendicular tread/riser intersection, removal of the cement/sand matrix was negligible, as observed in Figures 18 and 19. This indicates that the riser/tread intersection of the concrete unit is its most sheltered region, yielding relatively low concrete abrasion rates.

Figure 18. Negligible abrasion damage at riser/tread interface.

Figure 19. Riser/tread interface after severe abrasion of nosing.

This trend is attributable to the relationship between the geometry of the concrete surface with beach sediment size. Due to the perpendicular tread/riser intersection and the fact that the average value of D50 of the beach sediments in Table 1 is 26 mm, this suggests that there is no exposure to abrasion damage for approximately 13 mm widths, as both the tread and riser in this zone are not exposed to abrasion action at the initial stages. Figure 20 illustrates the interaction using an idealised spherical abrasive sediment. The 0.5D widths of the tread and riser are not immediately subjected to abrasion action.

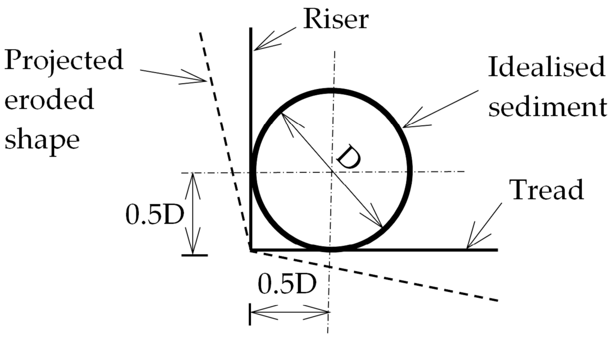

Figure 20. Schematic illustration of the scenario at the riser/tread interface.

Nevertheless, the progression of concrete material loss gradually exposes this region to interaction initially with small-sized sediments. The size and quantity of beach sediments abrading this region increases over time.

Moving seaward down the revetment, the severity of abrasion increased in row 3 and more so in row 4, shown in Figure 21 as manifested by the extensive exposure of coarse aggregates.

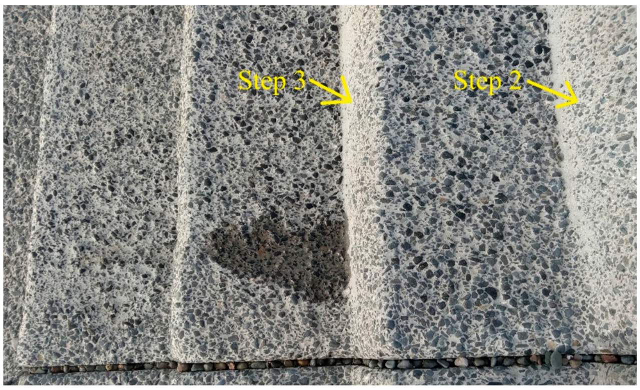

Figure 21. Severe abrasion damage at row 4 unit.

Figure 21 also indicates that the abrasion rate at the tread/riser intersection was relatively faster at the tread, as evidenced by the presence of a narrow width of intact cement/sand matrix at the base of the tread. The most severe damage appeared to be concentrated in the units located in rows 4 and 5, as shown in Figure 22.

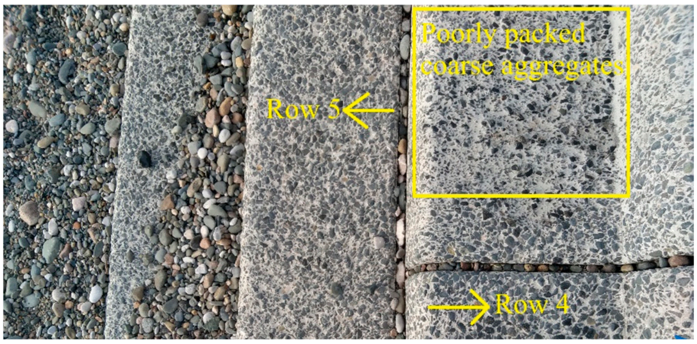

Figure 22. Abrasion damage at interface of row 4 and 5 units.

Figures 22 and 23 also suggest that the distribution of CA within concrete is a crucial factor for its abrasion performance. In a very few isolated spots, high localised abrasion rates were observed in surface zones with relatively sparse CA distribution. This can be attributed to CA grading, which resulted in inadequate particle packing in these zones. It should, however, be pointed out that these kinds of defects are normal in concrete works. Nevertheless, the findings indicated that the cement/sand matrix was wearing faster than the CA, thus implying that its Mohs hardness value (MH) was less than that of the CA used. The CA was classified as hornfels, with a MH of approximately 7 [28] and a micro-Deval number of 7 [4]; this hardness is comparable with the other igneous and metamorphic rock types present among the shingle, and the full details of the concrete mixture used in the revetment units at Cleveleys can be found in [4,22,28]. In fact, even within zones of dense CA packing, it was still apparent that due to differential wear in the two concrete phases, the CA formed roughness crests of the abraded surfaces. This is consistent with the observations made by Omoding et al. [28] on samples of a similar mixture abraded in the laboratory using the ASTM C1138 [12] test method. Therefore, these findings underscore the significance of CA grading in the achievement of economic abrasion-resistance concrete through dense packing of particles and corroborate the findings of Cunningham et al. [4].

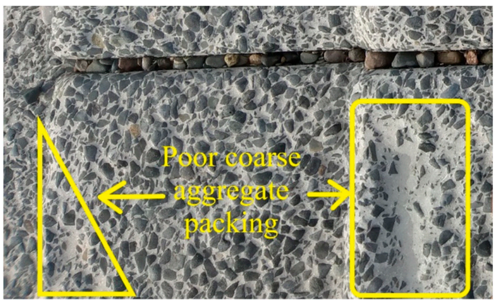

Figure 23. Abrasion damage of the cement/sand matrix at row 4.

4.1.2. Concrete Abrasion Mechanisms

A detailed visual inspection of damaged concrete surfaces revealed that the texture of the CA and cement/sand matrix surfaces was smooth. Further, craters were absent from damaged surfaces. These two observations point to absence of both CA plucking and cutting mechanisms in the removal of concrete by beach sediments. Based on the nature of the damaged surfaces described, it would appear that the dominant material removal mechanism at Cleveleys is by grinding/polishing. Such a response by the concrete surface is attributable to either the behaviour of the concrete material and/or modes of motion of the abrasive sediments. In the former case, it implies that the interfacial transition zone (ITZ) and bulk matrix of the concrete mixture has exhibited strength sufficient to resist the plucking of the CA that would have exacerbated the rate of material loss. In the latter case, it would suggest the absence of saltation or bouncing modes, whose impact results in cracking of the concrete, with material removal occurring when horizontal and vertical cracks intersect, as discussed in Omoding et al. [7].

Despite the observed type of wave breaking at the site being predominantly plunging, from the evidence of the damaged surface texture, the primary mode of motion of the abrading sediments was likely by rolling and/or sliding. However, this aspect needs verification through laboratory experiments. This is because whilst it is fairly well understood that the vortices generated by plunging and breaking can be capable of stirring up beach sediments into suspension [43], the precise motion of the coarse bed and suspended load on stepped and sloping concrete surfaces under breaking wave conditions requires further investigation.

4.1.3. Effect of Timber Groynes

Figure 24 shows the influence of timber groynes on observed concrete abrasion patterns. There is accretion of beach sediments on the left-hand side of the groyne in Figure 24a, whilst the beach level was lower by approximately 1 m elsewhere, as shown in Figure 24b. Regardless of the variations in beach levels, consistency in abrasion patterns was observed at the two locations in that the groyne occluded the regions of steps immediately behind its origin from interacting with beach sediments. As a result, the observed abrasion in these areas was lower relative to surfaces on either side of the groyne. In particular, the damage appeared more severe in the region between the groynes and spine beams. This indicates that the interaction of the sediments with the concrete surface was more intense in these constrained regions.

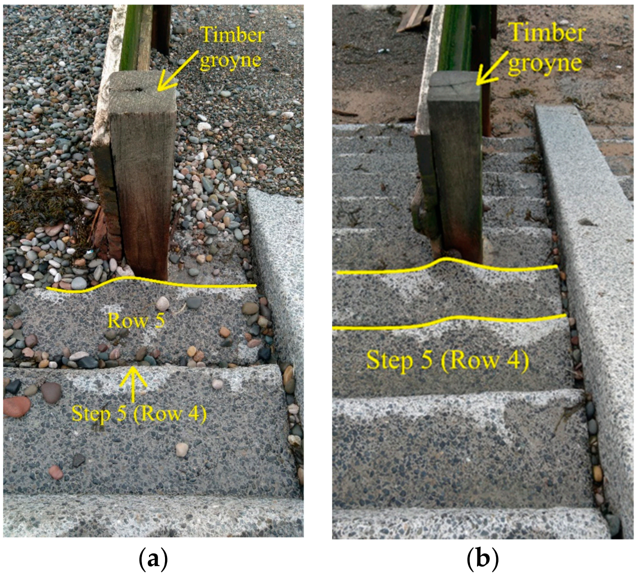

Figure 24. Impact of timber groynes on concrete abrasion damage, (**a**) area of significant shingle accretion (**b**) minimal shingle accretion.

However, the hydraulically aggressive environment in the surf zone currently makes it difficult to examine the modes of motion of beach sediments on the actual concrete surface to test this hypothesis.

4.2. Terrestrial Laser Scanning

One of the objectives of this campaign was to examine the feasibility of using terrestrial laser scanning (TLS) to reliably measure concrete abrasion rates in field conditions by sampling three locations along the revetment. Moreover, since the 3D laser scanner captured a portion of the beach, the relationship between beach levels and observed abrasion patterns was also assessed. However, it should be stated that beach levels vary throughout the year. The locations of the regions scanned are presented in Appendix A (Figure A1).

4.2.1. Concrete Abrasion Measurements

The concrete abrasion depths from the TLS workflow discussed in Section 4 are presented in Figures 25–27, while the distributions of abrasion depths are shown in Figures 28–30. Figures 25–27 show that TLS provided a dense cloud of data points, particularly at locations Q and R, that enabled detailed reconstruction of the abraded surfaces. The point cloud captured also enabled deduction of abrasion patterns that were consistent with field observations in that abrasion rates were highest at the nosings of the steps of concrete armour units. The density of points at location P was less than at location R despite having the same number of scan stations (five). This was caused by a low degree of overlap between the five scans at this particular location.

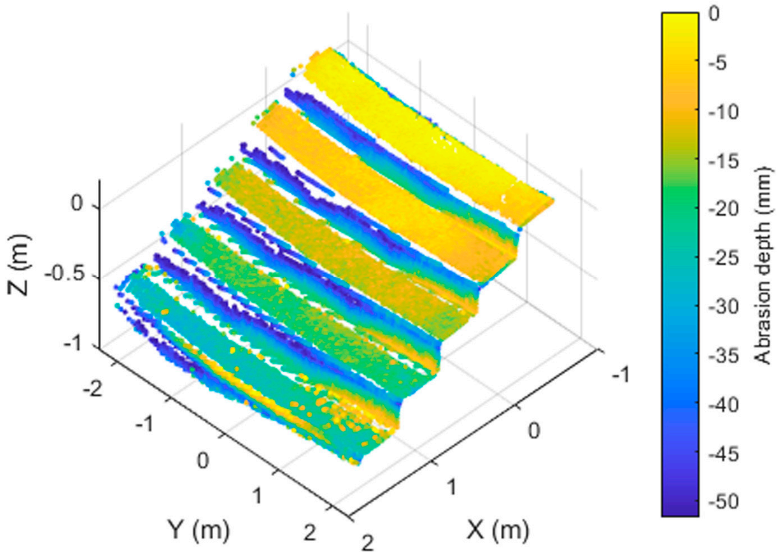

Figure 25. Concrete abrasion depths at location P.

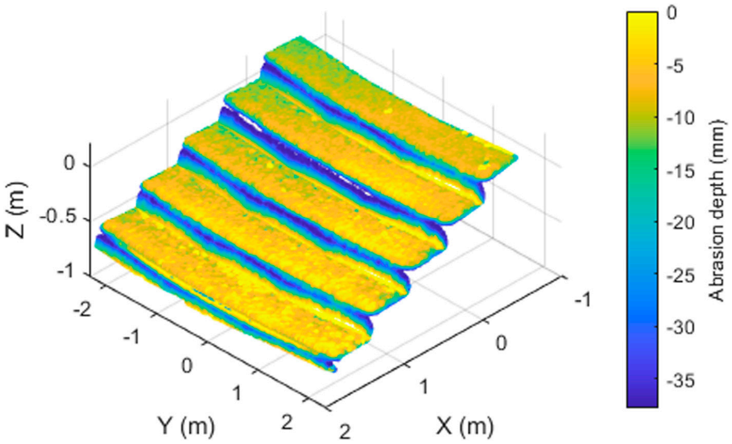

Figure 26. Concrete abrasion depths at location Q.

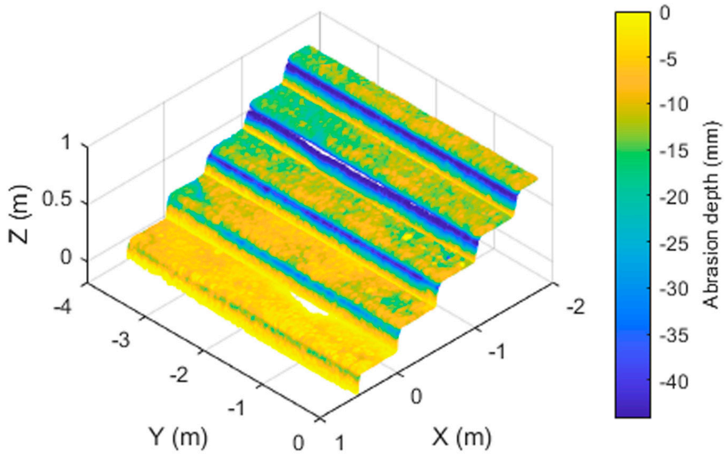

Figure 27. Concrete abrasion depths at location R.

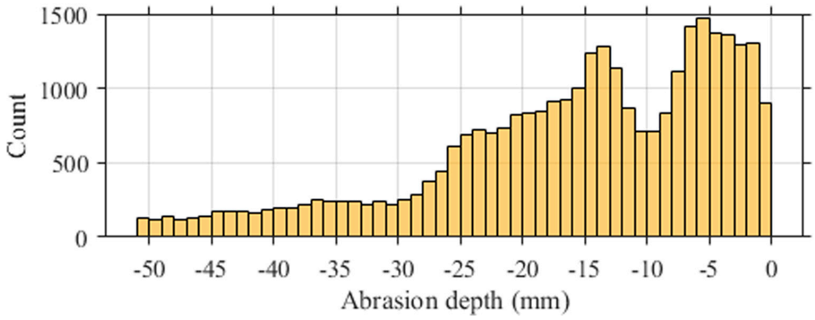

Figure 28. Distribution of abrasion depths at location P.

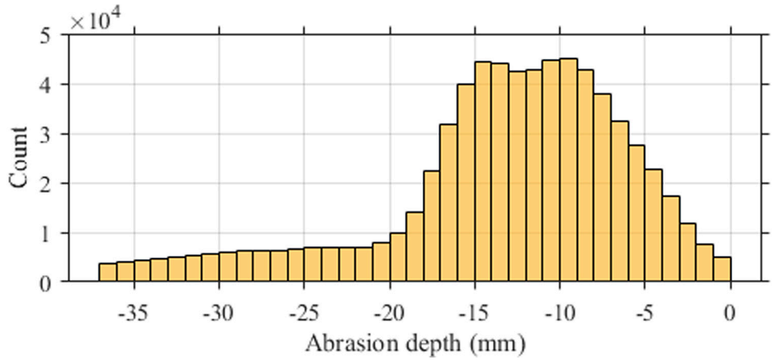

Figure 29. Distribution of abrasion depths at location Q.

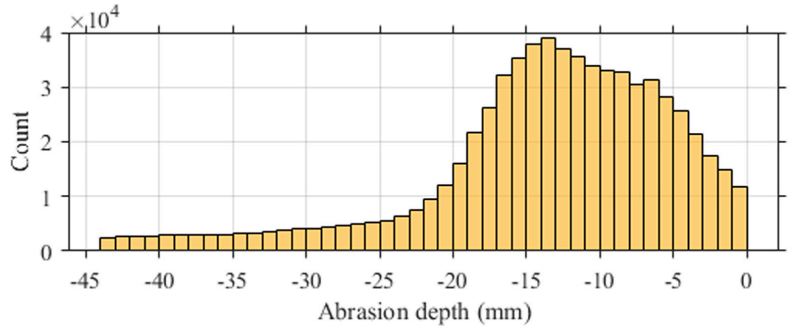

Figure 30. Distribution of abrasion depths at location R.

It can be observed in Figures 28–30 that a majority of abrasion depths measured at locations P, Q, and R were within 30, 20, and 25 mm, respectively. In fact, while the maximum abrasion depths at locations P, Q, and R were 52, 38, and 44 mm, respectively, the corresponding average values were 16, 13, and 14 mm. The trend in the distribution of abrasion depths at these locations is consistent throughout the three locations in that there was a significant decay in the number of abrasion depth values exceeding 30, 20, and 25 mm, respectively. From the exposure durations estimated from unit installation dates, the maximum abrasion values translate into rates of 4.0, 3.5, and 4.5 mm/year at locations P, Q, and R, respectively.

The concrete abrasion rates obtained in this study appear to be consistent with those presented by Allen and Terret [8] for sloping test panels constructed at Fleetwood, which is just north of the current site. This is because, despite the use of different concrete mixtures and revetment geometry, the field study [8] reported concrete abrasion rates of 2 to 13 mm/year, and findings of the present investigation fall within this range. It was also useful to compare the field concrete abrasion results obtained with those of the same concrete mixture abraded in the ASTM C1138 test. Omoding et al. [28] reported the 72-h abrasion loss of that concrete mixture as 2.48%, which translates to an average abrasion depth of 2.5 mm. This shows that, thus far, the average abrasion depth in the field for the period of about 11 years is approximately six times the 72-hour ASTM C1138 abrasion loss.

4.2.2. Comparison of TLS and Manual Measurements

This study also accessed the abrasion data collected during monitoring by Wyre Council over four phases consecutively carried out on 13th August 2011, 19th August 2011, 18th January 2012, and 9th July 2012. The method adopted involved using a steel template measuring gauge presented in Figure 31, which measured concrete abrasion at locations marked 1 to 6. The details of revetment locations monitored and the method description are provided in Appendix A.

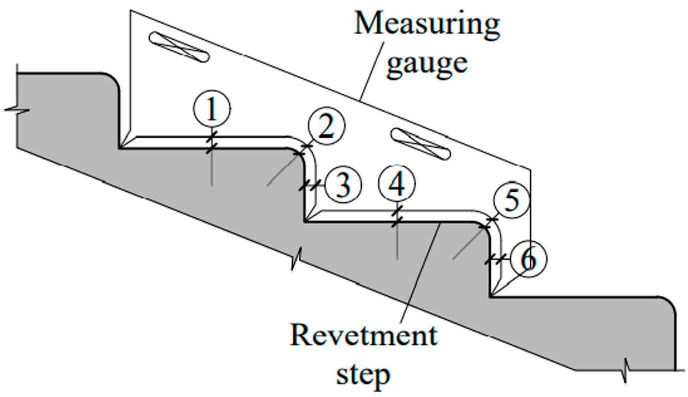

Figure 31. Steel template for abrasion monitoring in stepped concrete surfaces.

For purposes of this comparison, the findings of phases 2 and 4 monitoring conducted after exposure durations of 4 to 5.4 years and 4.9 and 6.3 years, respectively, were considered. Figures 32 and 33 present concrete abrasion rates obtained during these phases at step locations 1–6, defined in Figure 31b, whereby the negative values denote a reduction in surface elevation and vice versa. The units monitored for locations A to E and F to G are situated on rows 4 and 5, respectively.

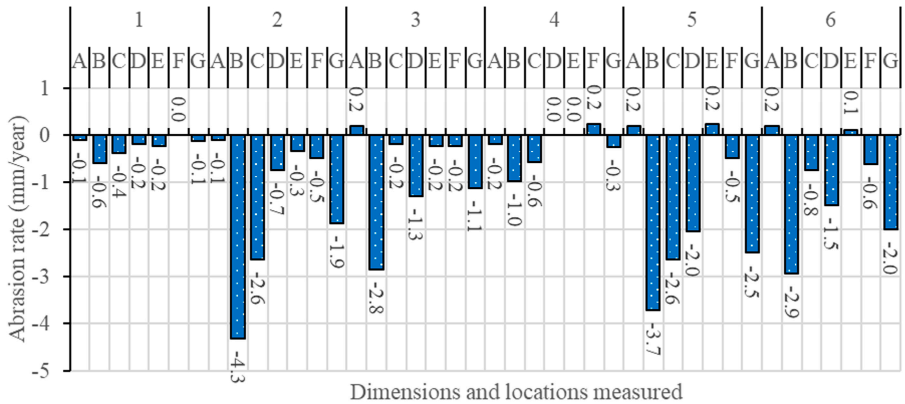

Figure 32. Abrasion rates obtained during phase 2 of Wyre Council monitoring.

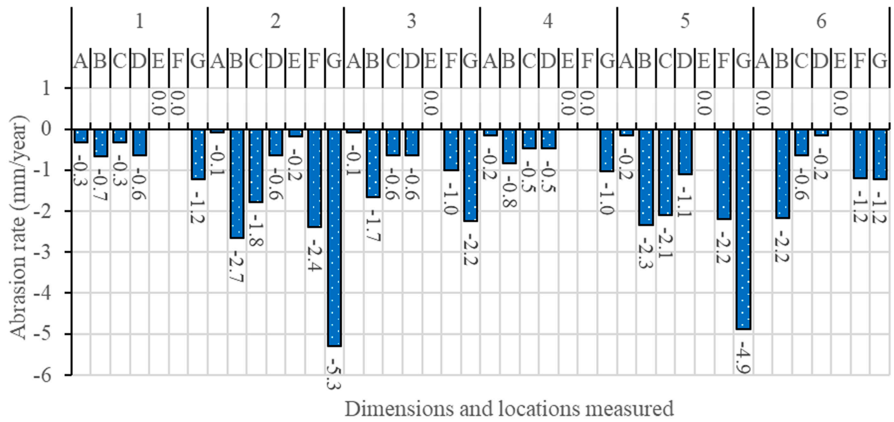

Figure 33. Abrasion rates obtained during phase 4 of Wyre Council monitoring.

Figure 33 shows that concrete abrasion rates ranged from 0 to 5.3 mm/year. The highest rates of 4.9 and 5.3 mm/year were at positions 5 and 2 of the steps, respectively, both on a unit marked G. The same trend was also observed in Figure 32, whereby the highest rates of 3.7 and 4.3 mm/year were again observed at positions 5 and 2, respectively, albeit both being at a different location, B. The fact that, in both cases, abrasion rates were consistently highest at the nosings of the steps is in agreement with the findings of both visual observations and TLS. Further, the maximum abrasion rates obtained from TLS that ranged from 3.5 to 4.5 mm/year are comparable to those obtained by the manual method, particularly during phase 2. This demonstrates the reliability of the TLS approach for concrete abrasion measurement. The relatively high abrasion rates obtained from manual monitoring can be attributed to sediments mainly abrading the cement/sand matrix in the initial period after installation and before full exposure of the relatively hard coarse aggregates. Other factors that could have contributed to the slight variations in the results include changes in wave characteristics and beach levels, which impact both wave breaking and littoral drift. It is also important to note that some of the results of phase 2 monitoring indicated that the post-exposure concrete surface elevation had marginally increased. This casts some doubt on the accuracy of the method used for measuring short-term concrete abrasion.

In summary, coastal revetment armour units may incorporate steps to increase surface roughness and mitigate overtopping and toe scour. Additionally, the steps also provide access to the beach for the residents and visitors [44]. If the rate of concrete abrasion (3.5 to 4.5 mm/year) at the locations investigated was to be at a steady state, the steps are likely to be completely removed from the units within a period of 40 to 50 years from the installation date. Thus, without carrying out routine repairs, the removal of steps (181 mm max. thickness perpendicular to the nosing) before the 100-year service life typically used in the design of U.K. major infrastructure, would result in the reduction of the proportion of wave energy dissipated by surface roughness and impaired access to the beach. However, whilst the loss of steps may reduce energy dissipation properties of the armour units, its consequences on the structural stability are insignificant over a service life of 50 or so years due to the 500 mm thick concrete waist slab adopted. Further, the contribution of the step to the stability of the armour unit would have been conservatively ignored in its design.

4.2.3. Relationship with Tide Levels

As already seen in Figure 5, the most abraded rows (4 and 5) are approximately between the MHWS and MHWN. More specifically, the severest damage was concentrated at the mid-region of the two rows, i.e., at approx. top and lower halves of rows 5 and 4, respectively. This finding is inconsistent with the general assertion by Thomas and Hall [45] that, in the case of seawalls, suitable conditions for significant abrasion by wave-driven solids are present in regions beneath the MHWN. The fact that concrete units at Cleveleys on row 3 and to a lesser extent on row 2 also exhibited abrasive effects of wave-driven shingle confirms that for sloping revetments, and depending on site conditions such as beach levels, concrete elements situated above MHWS can also suffer abrasion damage, albeit to a lesser degree.

While abrasion damage below MHWS was attributable to the stirring up of beach shingle by vortices created by plunging-type breaking waves at the vicinity of the revetment, the mild surface damage at locations above MHWS is likely due to the availability of sufficient wave energy capable of moving shingle up and down the swash zone. Therefore, based on the severity of abrasion damage, it is evident that for the coastal defences at Cleveleys, the motion of beach sediments and consequently their interaction with the concrete surface is more intense within the zone located between MHWS and MHWN.

4.2.4. Relationship with Beach Levels

Invariably, beach levels change throughout the year. Even so, TLS also captured beach levels near the revetment armour units assessed. These were used to evaluate the relationships between locations of the most abraded revetment units and beach levels. To that end, for the three locations scanned, cross-sections of 50 mm widths were taken through the point cloud of the entire concrete unit width to incorporate the beach profile. These sections were taken at or near the mid-length of the unit. Figures 34–36 show the relationships between the scanned revetment unit and the level of the beach.

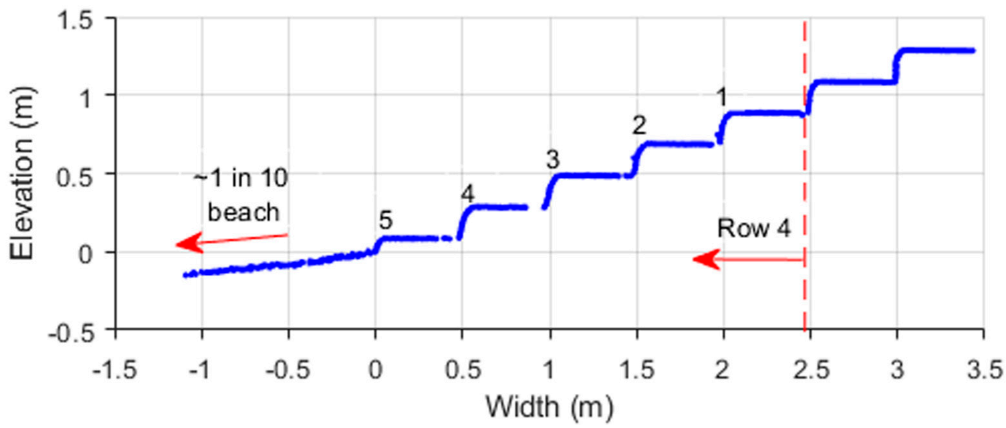

Figure 34. Relationship between beach and scanned armour unit at location P.

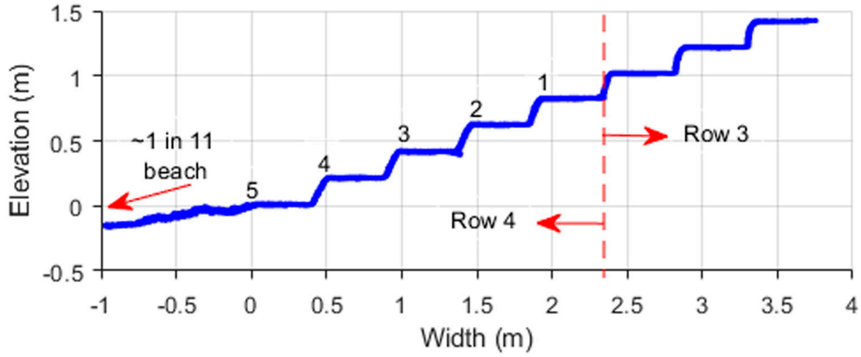

Figure 35. Relationship between beach and scanned armour unit at location Q.

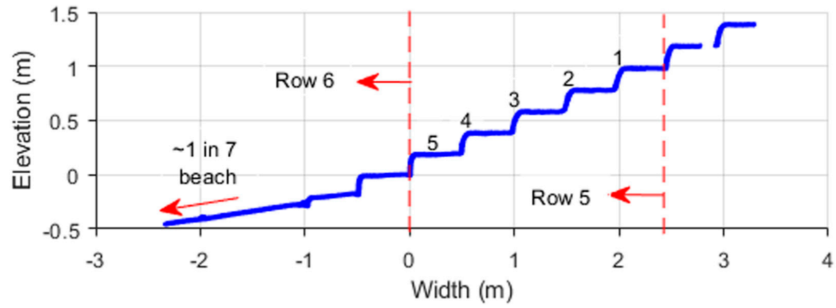

Figure 36. Relationship between beach and scanned armour unit at location R.

The results in Figures 34–36 show that at location R, the beach level interfaced with the revetment at approximately the mid-height of the second riser of the unit on row 6. In contrast, at location Q, the beach level was relatively higher, as it was near the mid-height of the fifth riser of row 4. In location P, the beach level was also at approximately the mid-height of the fifth riser of row 4.

Based on the findings of the TLS carried out on 21st May 2019, it is evident that the beach levels did not significantly differ from those visually observed during the site reconnaissance survey on 25th April 2019. Further, a qualitative inspection of the orientation (slopes) of the risers of the abraded steps indicated that the abrasion damage was more prominent in the revetment rows adjacent to the beach lines. As such, in location R, a relatively small degree of abrasion damage was observed in the two exposed steps of row 6 in comparison to row 5.

Thus, it would appear that the highest abrasion damage of the concrete revetments at Cleveleys occurred in the units directly at beach level. According to Thomas and Hall [45], sea walls also present similar results. In the case of stepped revetment armour units, the risers and treads of the steps exhibited outward and inward inclinations, respectively, because of wear, as highlighted in Figures 34–36. Further, although the influence of this scenario depends on the duration for which the reported beach levels remain more or less constant and the penetration depths of vortices, particularly due to plunging waves, it is plausible to suggest that the concrete units in row 6 are less likely to suffer severe abrasion damage. This is because of the sheltering effect provided by beach sediments, which suffer self-abrasion, as discussed by Dornbusch [46], while shielding concrete surfaces. However, the degree of sheltering will greatly depend on the depth of the submerged beach that is mobile during the tide.

5. Conclusions and Recommendations

This paper has presented a case study of concrete abrasion by shingle transported by breaking waves at Cleveleys on the Fylde coast of the U.K. It first examined the study site considering the hydrodynamic exposure conditions, design, and construction of stepped armour units and abrasion patterns exhibited. Thereafter, the feasibility of using terrestrial laser scanning (TLS) to measure abrasion in field conditions was examined, followed by an evaluation of damage recorded by TLS. The abrasion rates obtained from TLS were compared with the findings of the manual monitoring campaign undertaken by the asset owner, Wyre Council. Based on the study findings, the following conclusions are drawn:

1. The mechanism of concrete material loss is by polishing/grinding action based on the absence of craters, which typically result from the plucking of coarse aggregates. Therefore, the strength of the interfacial transition zone (ITZ) and bulk matrix ensures that the exposed coarse aggregates (CA) remain well anchored into the matrix. The smooth texture exhibited by both exposed CA and abraded matrix suggests that the predominant mode of shingle motion on the concrete surface is by rolling and/or sliding;
2. Terrestrial laser scanning (TLS) provides a dense cloud of 3D points that adequately define the topography of the abraded surface. These data can be processed using a combination of open-source and commercially available software to determine the depths of concrete abrasion damage with a reasonable degree of accuracy. The patterns of abrasion damage obtained from TLS are consistent with visual observations;
3. The maximum concrete abrasion rates range from 3.5 to 4.5 mm/year, and these rates are applicable to the nosings of the steps. The progression of the abrasion damage is such that the inclination of the risers increases outwards (clockwise) from the initially vertical orientation, whilst the wear of the treads progresses in the anti-clockwise direction about the tread/riser intersection. These directions apply when moving from south to north. It should be stated that the quoted rates are specific to the characteristics of the location and type of concrete adopted;
4. The shingle beach interfaced with concrete armour units within/near the region between the MHWS and MHWN, and the zone of the revetment with severe concrete abrasion is immediately after the line of this interface;
5. There is need for further research to experimentally examine the motion of shingle fronting stepped and non-stepped sloping revetments under breaking wave conditions.

Author Contributions: Conceptualization, N.O. and L.S.C.; methodology, N.O. and L.S.C.; software, N.O. and M.O.; validation, N.O., L.S.C. and M.O.; formal analysis, N.O. and L.S.C.; investigation, N.O., L.S.C., M.O. and B.F.; resources, N.O., L.S.C., G.F.L.-S. and B.F.; data curation, N.O. and L.S.C.; writing—original draft preparation, N.O. and L.S.C.; writing—review and editing, N.O., L.S.C., G.F.L.-S., M.O. and B.F.; visualization, N.O.; supervision, L.S.C. and G.F.L.-S.; project administration, N.O.; funding acquisition, L.S.C. All authors have read and agreed to the published version of the manuscript.

Funding: This research was funded by The University of Manchester, Department of Mechanical, Aerospace and Civil Engineering, Technical Ph.D. Scholarship.

Institutional Review Board Statement: Not applicable.

Informed Consent Statement: Not applicable.

Data Availability Statement: The data from this study can be obtained from the corresponding author by reasonable request.

Acknowledgments: The work presented here is part of wider research project by the authors. The authors wish to express their gratitude and sincere appreciation to the Department of Mechanical, Aerospace, and Civil Engineering (MACE) at The University of Manchester for funding this research and Mojgan Mosleh Hadi (Department of MACE) for provision of the 3D Laser Scanner. The authors are also grateful to Mike Wilkinson of Wyre Council for his advice and provision of the manually measured field data. Following the untimely passing of our colleague Mike Pomfret, CEng, CMgr, CEnv, FICE, FAPM, FCMI, FCIArb, and in recognition of his major contribution to Coastal Engineering on the Fylde Coast, the authors wish to dedicate this paper to his memory.

Conflicts of Interest: The authors declare no conflict of interest.

Appendix A

Appendix A.1. Field Investigation Details

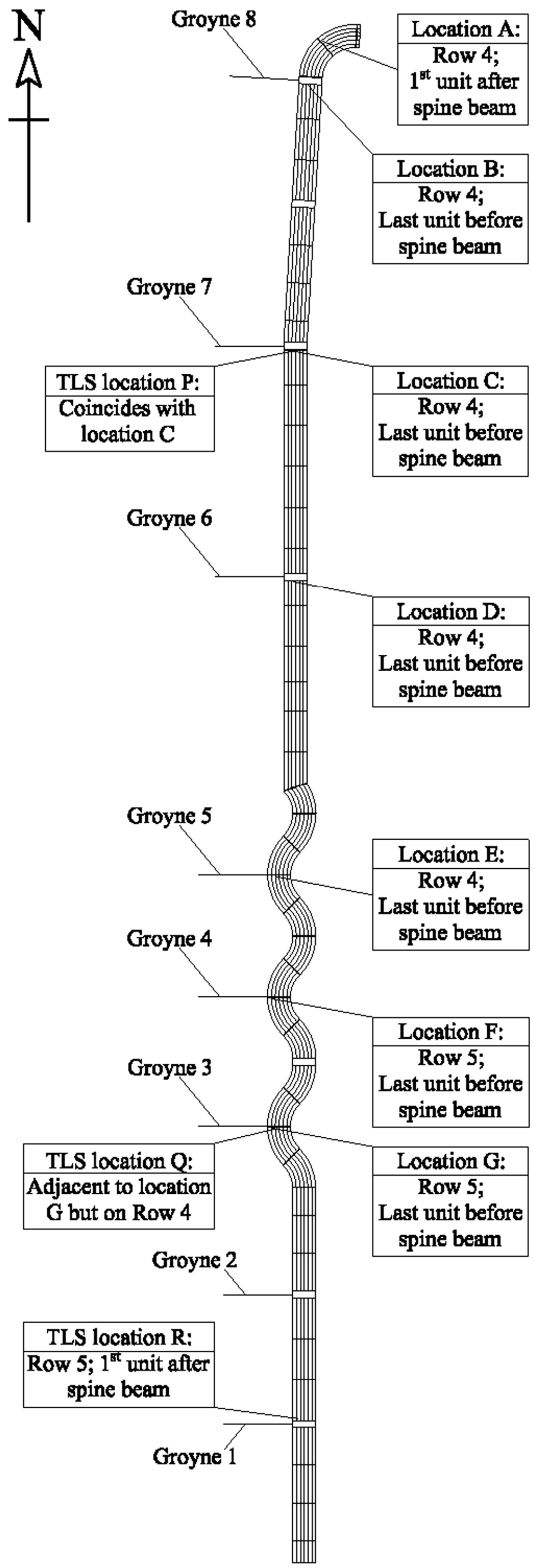

Figure A1. Plan of the location assessed by TLS and manually monitored.

Table A1. Description of concrete surfaces assessed during manual monitoring.

Location	Description	Installation Period
A	Row 4, 50 mm offset from edge of unit adjacent to spine beam, hence a relatively sheltered location.	August 2006
B	Raw 4, 50 mm offset from edge of unit adjacent to the spine beam, hence a very exposed location.	July 2006
C	Raw 4, 50 mm offset from edge of unit adjacent to the spine beam, hence a very exposed location.	May 2006
D	Raw 4, 50 mm offset from edge of unit adjacent to the spine beam, hence a very exposed location.	March 2006
E	Row 4, 0.5 mm offset from edge of unit adjacent to spine beam; relatively sheltered location (by groyne).	April 2007
F	Row 5, 0.5 mm offset from main timber plank face of groyne panel adjacent to spine beam/groyne; extremely exposed location.	July 2007
G	Row 5, 0.5 mm offset from main timber plank face of groyne panel adjacent to spine beam/groyne; extremely exposed location.	August 2008

Appendix A.2. Description of the Method for Manual Field Abrasion Monitoring

The manual method of concrete abrasion measurement utilised a steel monitoring template shown in Figure 31, a tape measure, and a mason's spirit level. This approach is specifically suited for stepped surfaces and considers the riser-tread interfaces of the steps as local benchmarks. It assumes that these interfaces are not abraded by sediments, thus providing suitable reference points for measuring concrete abrasion. To measure abrasion in the concrete steps, a gap between the template and existing concrete surfaces was first measured at selected reference units for each location (A–G). The reference units refer to those that are not often reached by the tide and are thus not abraded. The row one (1) units were generally used as references for all monitoring locations with the exception of D, in which a unit on row two (2) was used. Measurements from the reference units yielded gaps widths, Di, at points i = 1, 2 . . . and 6, as illustrated in Figure 31b. The same procedure was repeated at abraded locations of interest to obtain gaps widths, Xi, at surface points i = 1, 2 . . . and 6. The depth of concrete abrasion loss in the steps, Zi, was computed as Zi = Di − Xi. Concrete abrasion was measured after exposure durations ranging from 3.4 to 6.3 years, as shown in Table A2.

Table A2. Ages of the units during the abrasion monitoring by Wyre Council.

Location	Exposure Duration (Years)			
	Phase 1	Phase 2	Phase 3	Phase 4
A	4.4	5.0	5.4	5.9
B	4.5	5.1	5.5	6.0
C	4.7	5.3	5.7	6.2
D	4.8	5.4	5.8	6.3
E	3.8	4.3	4.8	5.3
F	3.5	4.1	4.5	5.0
G	3.4	4.0	4.4	4.9

Table A3. Specification of the Leica P40 ScanStation [39].

Measurement Method	**Ultra-High-Speed Time-of-Flight + Wave-Form-Digitising (WFD) Technology**
User interface	Full on-board scan control with full-colour touch screen
Data storage capacity	256 GB internal solid-state drive (SSD) or external USB devise
Scan range and reflectivity	Minimum: 0.4 m; maximum with reflectivity: 120 m (8%); 180 m (18%); 270 m (34%).
Maximum scan rate	1,000,000 points per second
Three-dimensional position (point) accuracy	3 mm @50 m; 6 mm @100 m
Range accuracy	1.2 mm +10 ppm over full range
Angular accuracy	0.0022° horizontal; 0.0022° vertical
Field-of-view (horizontal x vertical)	360° horizontal; 290° vertical
Laser wavelength	1550 nm (invisible)/658 nm (visible)
Laser class	1 (in accordance with IEC 60825:2014)
Standard battery dimensions	40 mm (D) × 72 mm (W) × 77 mm (H)
Standard battery weight	0.4 kg per battery
Standard battery capacity	Internal > 5.5 h (2 batteries)External > 7.5 h (room temp)
Scanner dimensions	238 mm (D) × 358 mm (W) × 395 mm (H)
Scanner weight	12.25 kg

References

1. May, V.J.; Hansom, J.D. Introduction to coastal geomorphology of Great Britain. In *Coastal Geomorphology of Great Britain*; Joint Nature Conservation Committee: Peterborough, UK, 2003; pp. 1–30. [CrossRef]
2. Wentworth, C.K. A scale of grade and class terms for clastic sediments. *J. Geol.* **1922**, *30*, 377–392. [CrossRef]
3. Fuller, R.M.; Randall, R.E. The Orford Shingles, Suffolk, UK-Classic conflicts in coastline management. *Biol. Conserv.* **1988**, *46*, 95–114. [CrossRef]
4. Cunningham, L.S.; Farrington, B.; Doherty, A. Briefing: Abrasion performance of concrete in coastal structures. *Proc. Inst. Civ. Eng. Marit. Eng.* **2015**, *168*, 157–161. [CrossRef]
5. CIRIA. *Seawalls: Survey of Performance and Design Practice*; CIRIA: London, UK, 1985.
6. Bray, R.N.; Tatham, P.F.B. *Old Waterfront Walls: Management, Maintenance and Rehabilitation*, 1st ed.; E & FN Spon: London, UK, 1992.
7. Omoding, N.; Cunningham, L.S.; Lane-Serff, G.F. Review of concrete resistance to abrasion by waterborne solids. *ACI Mater. J.* **2020**, *117*, 41–52. [CrossRef]
8. Allen, R.T.L.; Terrett, F.L. Durability of concrete in coast protection works. In Proceedings of the 11th Conference on Coastal Engineering, London, UK, 16–20 September 1968; pp. 1200–1210.
9. Van Wellen, E.; Chadwick, A.J.; Mason, T. A review and assessment of longshore sediment transport equations for coarse-grained beaches. *Coast. Eng.* **2000**, *40*, 243–275. [CrossRef]
10. Kryžanowski, A.; Mikoš, M.; Šušteršic, J.; Ukrainczyk, V.; Planinc, I. Testing of concrete abrasion resistance in hydraulic structures on the Lower Sava River. *Stroj. Vestn. J. Mech. Eng.* **2012**, *58*, 245–254. [CrossRef]
11. Liu, T.C. Abrasion resistance of concrete. *ACI J.* **1981**, *78*, 341–350.
12. *ASTM C1138*; Standard Test Method for Abrasion Resistance of Concrete (Underwater Method). ASTM International: West Conshohocken, PA, USA, 2012.
13. Hasan, M.S.; Li, S.S.; Zsaki, A.M.; Nokken, M.R. Measurement of abrasion on concrete surfaces with 3D scanning technology. *J. Mater. Civ. Eng.* **2019**, *31*, 04019207. [CrossRef]
14. Choi, S.; Bolander, J.E. A topology measurement method examining hydraulic abrasion of high workability concrete. *KSCE J. Civ. Eng.* **2012**, *16*, 771–778. [CrossRef]
15. Gyetvai, N.; Truong-Hong, L.; Laefer, D.F. Laser scan-based structural assessment of wrought iron bridges: Guinness Bridge, Ireland. *Proc. Inst. Civ. Eng. Eng. Hist. Herit.* **2018**, *171*, 76–89. [CrossRef]

16. Omer, M.; Margetts, L.; Mosleh, M.H.; Cunningham, L.S. Inspection of concrete bridge structures: Case study comparing conventional techniques with a Virtual Reality approach. *J. Bridge Eng.* **2021**, *26*, 05021010. [CrossRef]
17. Mizoguchi, T.; Koda, Y.; Iwaki, I.; Wakabayashi, H.; Kobayashi, Y.; Shirai, K.; Hara, Y.; Lee, H.S. Quantitative scaling evaluation of concrete structures based on terrestrial laser scanning. *Autom. Constr.* **2013**, *35*, 263–274. [CrossRef]
18. Olsen, M.J.; Kuester, F.; Chang, B.J.; Hutchinson, T.C. Terrestrial laser scanning-based structural damage assessment. *J. Comput. Civ. Eng.* **2010**, *24*, 264–272. [CrossRef]
19. Van Gosliga, R.; Lindenbergh, R.; Pfeifer, N. Deformation analysis of a bored tunnel by means of terrestrial laser scanning. *Int. Arch. Photogramm. Remote Sens. Spat. Inf. Sci. ISPRS Arch.* **2006**, *36*.
20. Xie, X.; Lu, X. Development of a 3D modeling algorithm for tunnel deformation monitoring based on terrestrial laser scanning. *Undergr. Space* **2017**, *2*, 16–29. [CrossRef]
21. Milenkovic, M.; Pfeifer, N.; Glira, P. Applying terrestrial laser scanning for soil surface roughness assessment. *Remote Sens.* **2015**, *7*, 2007–2045. [CrossRef]
22. Omoding, N.; Cunningham, L.S.; Lane-Serff, G.F. Effect of using recycled waste glass coarse aggregates on the hydrodynamic abrasion resistance of concrete. *Constr. Build. Mater.* **2020**, *268*, 121177. [CrossRef]
23. Truong-Hong, L. Equipment Considerations for Terrestrial Laser Scanning for Civil Engineering in Urban Areas. *J. Sci. Res. Rep.* **2014**, *3*, 2002–2014. [CrossRef]
24. Lague, D.; Brodu, N.; Leroux, J. Accurate 3D comparison of complex topography with terrestrial laser scanner: Application to the Rangitikei canyon (NZ). *ISPRS J. Photogramm. Remote Sens.* **2013**, *82*, 10–26. [CrossRef]
25. Cunningham, L.; Robertshaw, G.; Pomfret, M. Blackpool central area coast protection scheme, UK. *Proc. Inst. Civ. Eng. Marit. Eng.* **2012**, *165*, 21–29. [CrossRef]
26. Cunningham, L.; Burgess, A. Design and construction of the tower headland wave walls, Blackpool, UK. *Proc. Inst. Civ. Eng. Civ. Eng.* **2012**, *165*, 171–178. [CrossRef]
27. *BS 6349-1-4*; Maritime Works: General—Code of Practice for Materials. British Standards Institution: London, UK, 2013.
28. Omoding, N.; Cunningham, L.S.; Lane-Serff, G.F. Influence of coarse aggregate parameters and mechanical properties on the abrasion resistance of concrete in hydraulic structures. *J. Mater. Civ. Eng.* **2021**, *33*, 04021244. [CrossRef]
29. Datewell, B.V. Directional Waverider MkIII, the Directional Waverider DWR-MkIII: Over Three Years of Continuous Operation. 2021. Available online: https://www.datawell.nl/Portals/0/Documents/Brochures/datawell_brochure_dwr-mk3_b-09-09.pdf (accessed on 1 December 2021).
30. Channel Coastal Observatory. Regional Coastal Monitoring Programmes, Waves: Site Reports. 2020. Available online: https://www.channelcoast.org/reports/ (accessed on 1 December 2020).
31. National Tidal and Sea Level Facility. Liverpool Tide Gauge Site. 2020. Available online: https://ntslf.org/tgi/portinfo (accessed on 1 December 2021).
32. Davies, J.L. A morphogenic approach to world shorelines. *Z. Fur Geomorphol.* **1964**, *8*, 127–142. [CrossRef]
33. Miles, A.; Ilic, S.; James, M.R.; Whyatt, D. Morphological evolution around a groyne structure at Cleveleys. In Proceedings of the Coastal Dynamics, Arcachon, France, 24–28 June 2013; Coastal Dynamics: Arcachon, France, 2013; pp. 1195–1206.
34. Ellis, C. *The Pebbles on the Beach*, 1st ed.; Faber and Faber Limited: London, UK, 1965.
35. Wilson, A.A.; Evans, W.B. *Geology of the Country Around Blackpool*, 1st ed.; British Geological Survey: London, UK, 1990. Available online: https://pubs.bgs.ac.uk/publications.html?pubID=B01533 (accessed on 1 December 2021).
36. *BS EN 933*; Tests for Geometrical Properties of Aggregates. Part 1: Determination of Particle Size Distribution-Sieving Method. British Standards Institution: London, UK, 2012.
37. Rogers, J.; Hammer, B.; Brampton, A.; Challinor, S.; Glennerster, M.; Brenton, M.P.; Bradbury, A. *Beach Management Manual*, 2nd ed.; CIRIA: London, UK, 2010.
38. De Algeria Arzaburu, A.R.; Ilic, S.; Gunawardena, Y. A Study of intertidal bar dynamics using the Argus video system. In Proceedings of the Sixth International Symposium on Coastal Engineering and Science of Coastal Sediment Process, New Orleans, LA, USA, 13–17 May 2007. [CrossRef]
39. Leica Geosystems. Leica ScanStation P30/P40. 2017. Available online: https://w3.leica-geosystems.com/downloads123/hds/hds/general/brochures-datasheet/Leica_ScanStation_P30-P40_Plant_DS_en.pdf (accessed on 1 December 2021).
40. Leica Geosystems. Leica Cyclone Register 360-3D Laser Scanning Point Cloud Registration Software. 2020. Available online: https://leica-geosystems.com/products/laser-scanners/software/leica-cyclone/leica-cyclone-register-360 (accessed on 1 December 2021).
41. Cloud Compare. 3D Point Cloud and Mesh Processing Software, Open Source Project. 2020. Available online: https://www.danielgm.net/cc/ (accessed on 1 December 2021).
42. *BS EN 1990*; Eurocode—Basis of Structural Design. British Standards Institution: London, UK, 2002.
43. Fredsoe, J.; Deigaard, R. *Mechanics of Coastal Sediment Transport*; Advanced Series on Ocean Engineering; World Scientific: London, UK, 1992; Volume 3. [CrossRef]
44. Kerpen, N.; Schlurmann, T. Stepped revetments-Revisited. In Proceedings of the 6th International Conference on the Application of Physical Modelling in Coastal and Port Engineering and Science (Coastlab16), Ottawa, Canada, 10–13 May 2016; pp. 1–10.

45. Thomas, R.S.; Hall, B. *Seawall Design*, 1st ed.; CIRIA: Oxford, UK, 1992.
46. Dornbusch, U.; Williams, R.B.G.; Moses, C.; Robinson, D.A. Life expectancy of shingle beaches: Measuring in situ abrasion. *J. Coast. Res.* **2002**, *255*, 249–255. [CrossRef]